Published online 19 May 2017

Nucleic Acids Research, 2017, Vol. 45, No. 12 ***7515–7526***
doi: 10.1093/nar/gkx465

Dynamics of sequestration-based gene regulatory cascades

Tatenda Shopera, William R. Henson and Tae Seok Moon*

Department of Energy, Environmental and Chemical Engineering, Washington University in St. Louis, St. Louis, MO, 63130, USA

Received December 31, 2016; Revised May 08, 2017; Editorial Decision May 09, 2017; Accepted May 10, 2017

ABSTRACT

Gene regulatory cascades are ubiquitous in biology. Because regulatory cascades are integrated within complex networks, their quantitative analysis is challenging in native systems. Synthetic biologists have gained quantitative insights into the properties of regulatory cascades by building simple circuits, but sequestration-based regulatory cascades remain relatively unexplored. Particularly, it remains unclear how the cascade components collectively control the output dynamics. Here, we report the construction and quantitative analysis of the longest sequestration-based cascade in *Escherichia coli*. This cascade consists of four *Pseudomonas aeruginosa* protein regulators (ExsADCE) that sequester their partner. Our computational analysis showed that the output dynamics are controlled in a complex way by the concentration of the unbounded transcriptional activator ExsA. By systematically varying the cascade length and the synthesis rate of each regulator, we experimentally verified the computational prediction that ExsC plays a role in rapid circuit responses by sequestering the anti-activator ExsD, while ExsD increases response times by decreasing the free ExsA concentration. In contrast, when additional ExsD was introduced to the cascade via indirect negative feedback, the response time was significantly reduced. Sequestration-based regulatory cascades with negative feedback are often found in biology, and thus our finding provides insights into the dynamics of this recurring motif.

INTRODUCTION

Biological systems use diverse regulatory strategies involving many interacting DNA sequences, RNAs and proteins to achieve robust dynamic control of gene expression (1). RNA regulation of physiological responses is ubiquitous in living cells and contributes to rapid cellular adaption to stress conditions (2). While small RNA regulators generate fast gene expression responses (3–6), protein–protein interactions also exhibit rapid responses when the protein regulators are already present in the cell (3). Negative feedback loops represent another widely found mechanism that natural biological systems employ to modulate gene expression dynamics. For instance, negative auto-regulation, in which a system's output molecule negatively regulates its own synthesis, speeds up the response time compared to its counterpart without negative feedback regulation (7). Regulatory mechanisms involving small RNAs, protein–protein interactions, and negative autoregulation enable biological systems to optimize gene expression in dynamic environments.

Regulatory cascades can generate precisely controlled gene expression dynamics in response to environmental signals (8). Ordered transcriptional activation has been shown in both prokaryotic and eukaryotic systems, which allows for optimal use of transcriptional resources (9–11). By building and characterizing synthetic regulatory cascades, Hooshangi *et al*. showed that the transcriptional cascade depth (i.e. the number of layers in a cascade) modulates the response time of gene expression (12). In addition, regulatory cascades that combine both transcriptional and translational regulation have been shown to control the dynamics of important cellular processes such as bacterial pathogenesis and biofilm production (13). Understanding the principles that govern the dynamic control of gene expression is necessary for predicting complex system-level behaviors and engineering robust gene expression dynamics for a wide range of biotechnological applications (14).

Protein sequestration is ubiquitous in biology (15), and sequestration-based gene regulatory cascades are frequently found in pathogenic bacteria (16–18). For example, through a partner-swapping mechanism, the ExsA–ExsD–ExsC–ExsE protein regulatory cascade provides precise control of the type III secretion system (T3SS) gene expression in *Pseudomonas aeruginosa*, an opportunistic pathogen. Considerable efforts have focused on elucidating the regulatory structure of the T3SS and its basic organization (19–23). A transcription factor (ExsA) activates the target promoter (20) and is sequestered by an anti-activator (ExsD) into an inactive ExsA–ExsD complex (21).

*To whom correspondence should be addressed. Tel: +1 314 935 5026; Fax: +1 314 935 7211; Email: tsmoon@wustl.edu

© The Author(s) 2017. Published by Oxford University Press on behalf of Nucleic Acids Research.
This is an Open Access article distributed under the terms of the Creative Commons Attribution License (http://creativecommons.org/licenses/by-nc/4.0/), which permits non-commercial re-use, distribution, and reproduction in any medium, provided the original work is properly cited. For commercial re-use, please contact journals.permissions@oup.com

A chaperone ExsC functions as an anti-anti-activator that sequesters ExsD into a complex (ExsD–ExsC) and liberates free ExsA, which activates the T3SS pathogenicity machinery (19). A fourth protein regulator (ExsE) sequesters ExsC into a complex (ExsC–ExsE). This mechanism prevents ExsC from interacting with ExsD until ExsE is exported from the cell (22,23).

Despite these advances in understanding the regulatory structure of the ExsADCE cascade, it is still unclear how the T3SS is timely activated and how each protein component contributes to the dynamics of the T3SS activation. A key challenge in quantitatively understanding the dynamics of the ExsADCE regulatory cascade is that the cascade is intricately integrated into the complex endogenous circuitries that respond to poorly defined environmental signals (24–29). In this work, we aim to determine how individual components of the ExsADCE regulatory cascade interact to affect gene expression dynamics. To achieve this goal, we decoupled the ExsADCE regulatory cascade from the poorly-understood native regulatory network of *P. aeruginosa*. Specifically, we constructed and characterized a synthetic ExsADCE regulatory cascade in *E. coli* in a piecewise fashion and determined the roles of each protein interaction and negative feedback in gene expression dynamics. Using this bottom-up approach that combines computational modeling and experiments, we found four key factors that determined the gene expression dynamics of the ExsADCE regulatory cascade: (i) the steady state free ExsA concentration, (ii) the apparent ExsD concentration (the initial free ExsD concentration of OFF-state cells), (iii) multi-member protein interactions in which the rapid response is mediated by ExsC and (iv) indirect negative feedback loops. In addition, we found that negative feedback loops embedded in the ExsADCE cascade enhance the robustness of gene expression dynamics.

MATERIALS AND METHODS

Strains and growth media

Escherichia coli DH10B (30) was used for all experiments. Cells were grown in filter-sterilized M9 minimal medium supplemented with 1.0 mM thiamine hydrochloride, 0.8 mM L-leucine, 0.2% (w/v) casamino acids, 0.4% (v/v) glycerol, 2.0 mM $MgSO_4$ and 0.1 mM $CaCl_2$. Kanamycin (20 μg/ml), ampicillin (100 μg/ml) and chloramphenicol (34 μg/ml) were added as appropriate. Three inducers were used at the following concentrations: Ara (Arabinose, 0 to 25 mM), aTc (anhydrotetracyline, 0–500 ng/ml), and 3OC6 (*N*-(β-ketocaproyl)-L-homoserine lactone, 0–5 μM). All the inducers and chemical reagents used in this study were purchased from Sigma-Aldrich (St. Louis, MO, USA) unless otherwise indicated.

Plasmid design and circuit construction

All the genetic circuits were constructed following the Golden-Gate DNA assembly technique (31) and using type IIS restriction enzymes (BspMI, BsaI, and BsmBI from New England Biolabs, Ipswich, MA, USA). The regulator gene *exsC*, the pLux* promoter, and the pBAD promoter used in this study were PCR amplified from pLux*-*exsC* and pBAD-*sicA** plasmids (32), using Phusion High-Fidelity DNA polymerase (New England Biolabs, Ipswich, MA). The pexsD-*gfp*, pexsD-*gfp*-*exsD* and pTet*-*exsD*-BBa_J23116-*exsA* plasmids had been previously constructed (33). The *exsE* gene was PCR-amplified and cloned from the genomic DNA of *P. aeruginosa* PAO1 (ATCC 47085). Genetic parts were ligated using T4 DNA ligase (New England Biolabs, Ipswich, MA). Constructed plasmid sequences were verified by DNA sequencing (PNACL, Washington University School of Medicine). Electro-competent *E. coli* DH10B was transformed with plasmids (Supplementary Table S8) using electroporation (Eppendorf Eporator), and frozen stocks were stored at –80°C (Supplementary Table S9). All the oligonucleotides were purchased from Integrated DNA Technologies (IDT, Coralville, IA, USA). All genetic part sequences used in this study are shown in Supplementary Table S10.

Fluorimetry

Cells were initially grown overnight (~16 h) at 37°C and 250 rpm in 5 ml of supplemented M9 media with 500 ng/ml aTc (OFF-state) and appropriate antibiotics. The overnight OFF-state cultures were centrifuged at 3000g for 5 min and resuspended in 5 ml of fresh supplemented M9 media three times. Next, cells were subcultured (1:100 dilution) in fresh supplemented M9 media (10 ml), grown for 1 h (37°C and 250 rpm), and transferred to fresh supplemented M9 media (0.6 ml) in deep 96-well plates (Eppendorf). Each culture (0.6 ml) was grown (37°C and 250 rpm) at inducer concentrations as indicated in Figure 1. After 8 h, cells were centrifuged and the cell pellet was re-suspended in 200 μl filtered 0.9% (w/v) saline (pH 8.0). The population level fluorescence measurements ($f_{GFP} = GFP/Abs_{600}$, where Abs_{600} and f_{GFP} respectively represent the absorbance value at 600 nm and GFP fluorescence per cell) were performed in a 96-well microplate (Chimney well and F-bottom, REF-655096, Grenier Bio-One) using a Tecan Infinite M200 PRO plate reader (GFP setting: excitation at 483 nm and emission at 530 nm). Autofluorescence ($f_{AGFP} = GFP/Abs_{600}$ of DH10B lacking GFP) was subtracted from f_{GFP} of all experimental samples.

Conversion of GFP arbitrary units into relative expression units (REUs)

Relative expression units (REUs) were calculated using DH10B cells containing a reference plasmid pAH016 (which has a constitutively expressed *gfp* gene; see Supplementary Table S8), which had been previously constructed (34). The objective of using REUs is to standardize measurements between labs and projects by normalizing measured fluorescence values to that of a reference *gfp* construct. Raw GFP values were converted into REU using the following formula: F_{GFP} (REU) = $[f_{GFP} - f_{AGFP}]/[f_{GFP\_pAH016} - f_{AGFP}]$, where f_{GFP}, f_{AGFP} and f_{GFP_pAH016} respectively represent GFP fluorescence per cell produced by experimental constructs, autofluorescence per cell (background fluorescence of DH10B cells lacking GFP), and GFP fluorescence per cell produced by the reference construct.

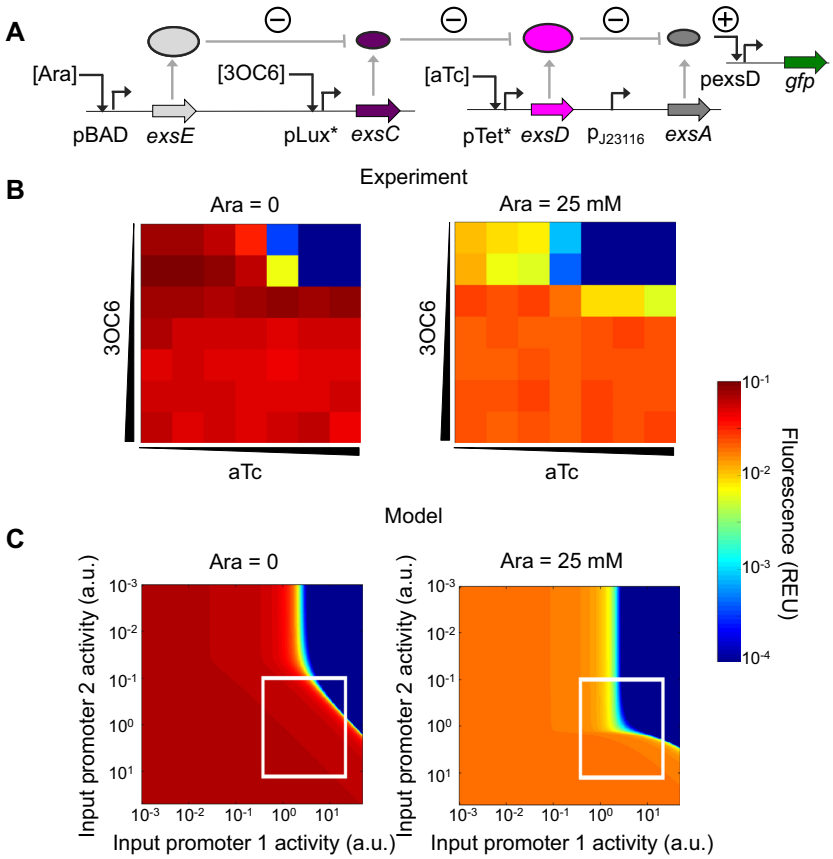

Figure 1. Construction and characterization of a synthetic ExsADCE regulatory cascade in *E. coli*. (**A**). Diagram of a synthetic ExsADCE regulatory cascade constructed in *E. coli*. A transcriptional activator ExsA activates its target pexsD promoter. An anti-activator ExsD sequesters ExsA into an inactive complex. A chaperone ExsC sequesters ExsD, releasing free ExsA. A fourth regulator ExsE sequesters ExsC into a complex. Here, **+** and **–** represent activating and repressing interaction, respectively. ExsA expressed from a constitutive promoter (pJ23116) controls *gfp* expression from the pexsD promoter. pTet* (aTc), pLux* (3OC6) and pBAD (Ara) control the expression of ExsD, ExsC and ExsE, respectively. (**B**). Fluorescence outputs determined experimentally. The experiments were performed at anhydrotetracycline (aTc) concentrations of 0, 0.0032, 0.016, 0.4, 2, 10 and 50 ng/ml; *N*-(β-ketocaproyl)-L-homoserine lactone (3OC6) concentrations of 0, 0.32, 1.6, 8, 40, 200 and 1000 nM; and arabinose (Ara) concentrations of 0 and 25 mM. Data are averages of experiments performed on three different days. (**C**). Computationally determined heat maps over a wide range of promoter activities (Supplementary Data). Note that the heat maps in Figure 1B and C cannot be directly compared due to rescaling of the axes from inducer concentrations to promoter activities. Supplementary Figure S1 shows a quantitative comparison (with an R^2 value of 0.93). Output values and input promoter activities are reported in relative expression units (REU) and arbitrary fluorescence units (a.u.), respectively. White boxes indicate the experimental ranges used in Figure 1B. Supplementary Table S11 shows $OD_{600\,nm}$ values for Figure 1.

Flow cytometry

Cells were initially grown overnight (~16 h) at 37°C and 250 rpm in 5 ml of supplemented M9 media with 500 ng/ml aTc (OFF-state) and appropriate antibiotics. The overnight OFF-state cultures were centrifuged at 3000g for 5 min and resuspended in fresh supplemented M9 media three times. Next, cells were subcultured (1:100 dilution) in fresh supplemented M9 media, grown for 1 h (37°C and 250 rpm), and transferred to fresh supplemented M9 media (0.6 ml) in deep 96-well plates (Eppendorf). Each culture (0.6 ml) was grown (37°C and 250 rpm) at inducer concentrations indicated in each figure. Samples were taken every 0.5 h and transferred to 200 μl filtered 0.9% (w/v) saline (pH 8.0) supplemented with 2.0 mg/ml kanamycin in 96-well assay microplates (U-bottom, REF-353910 from BD Biosciences, San Jose, CA, USA) for measurements. Flow cytometry analysis was carried out using a Millipore Guava EasyCyte High Throughput flow cytometer with a 488 nm excitation laser and a 512/18 nm emission filter. The flow rate was 0.59 μl/s. All data contained at least 5000 events gated by forward and side scatter. FlowJo (TreeStar Inc.) was used to obtain the arithmetic mean of the fluorescence distribution. Fluorescence (REU) was calculated using the following formula: $F_s = [F_{experiment} - F_{DH10B}] / [F_{control} - F_{DH10B}]$ where F_s, $F_{experiment}$, $F_{control}$ and F_{DH10B} respectively represent the reported sample fluorescence, measured sample fluorescence, measured fluorescence of the reference construct with constitutively expressed *gfp* (pAH016), and autofluorescence (background fluorescence of DH10B lacking GFP). Reported normalized fluorescence values were then calculated using the following formula: $F_{Normalized} = F_s/F_{smax}$ where F_{smax} represents the maximum sample fluorescence. Averages and SEM of the arithmetic means were obtained from replicates performed on different days as indicated.

Computational modeling

Because it is challenging to directly measure bound and unbound protein concentrations for multi-protein signaling cascades, protein concentrations were estimated using mathematical models that were fitted to response times which were calculated from GFP fluorescence time-course experiments (see Supplementary Data for modeling details). It is worth noting that the steady-state free ExsA concentrations used in this work are model-derived values that were obtained by considering experimentally measured parameters, typical parameters for bacteria, and physiologically relevant bacterial protein concentration ranges (13,15,33,35–39). Thus, the steady-state free ExsA concentrations are just reasonably estimated values, not accurate ones. To evaluate the validity of our modeling approach, we first compared model response times and experimentally determined response times (Supplementary Figure S7; $R^2 = 0.94$ with respect to the $y = x$ line). Additionally, the experimentally measured GFP fluorescence values were compared to model-derived steady state GFP values (Supplementary Figure S9; $R^2 = 0.89$ with respect to the $y = x$ line). These quantitative comparisons, which yield high R^2 values, indicate the validity of our modeling approach. All mathematical simulations were performed using MATLAB 2016a (Mathworks). Equations and derivations relevant to each figure can be found in the Supplementary Data.

RESULTS

Construction and characterization of a synthetic ExsADCE regulatory cascade in *E. coli*

The first step in this work was to build and characterize a genetic circuit with all four regulators (ExsADCE), the longest sequestration-based cascade constructed so far (Figure 1A). This quantitative characterization was performed by measuring the green fluorescence protein (GFP) output at steady state. This static information was obtained to confirm the expected functionality and interactions of each regulator in *E. coli* (a heterologous host) and to establish the basis of model parameters for later analyses of gene expression dynamics (see Supplementary Data for details). This circuit consists of *exsA*, *exsD*, *exsC* and *exsE* under the transcriptional control of pJ23116 (constitutive), pTet* (aTc-inducible), pLux* (3OC6-inducible), and pBAD (Ara-inducible) promoters, respectively. To measure the ExsADCE cascade output, *gfp* was fused to the pexsD promoter (33), which is activated by unbound free ExsA. As expected, low GFP levels were observed only when the aTc (ExsD) concentration is high and the 3OC6 concentration is low (Figure 1B). We also observed the expected result that ExsE reduced GFP outputs (Figure 1B and C; for the computational model, see Supplementary Data). Previously, we demonstrated that ExsC functions as a tuning knob, which allows for fine-tuning of the gene expression output (33). These results demonstrate that ExsE functions as an additional tuning knob, an important feature of the complex ExsADCE regulatory cascade that enables optimal control of gene expression.

Modeling dynamics of the ExsADCE cascade

To determine how the multi-member protein–protein interactions in the ExsADCE cascade impact the gene expression dynamics, we developed computational models (Supplementary Data). The first model describes a simple circuit consisting of only the ExsA regulator and its target promoter pexsD. Interestingly, our computational simulation showed that the target gene expression response time (i.e. the time to reach 50% of the steady-state gene expression level; Figure 2A) is dependent on the steady-state free ExsA concentration. Specifically, the response time can be either decreased or increased based on the steady-state free ExsA concentration regime (Figure 2B). Our computational model revealed two regimes: the first regime is at lower ExsA concentrations, where the response time increases with the steady-state free ExsA concentration, and the second regime is at higher ExsA concentrations, where the response time decreases with the concentration (Figure 2B). The increasing trend in the first regime can be attributed to the increasing 'achievable maximum' pexsD output (A/K) when the free ExsA concentration (A) is much lower than the half maximal constant (K) of the pexsD promoter (here, normalized pexsD output $= A/[A + K]$). In this regime, an increase in A will require more time to reach $A/2K$. In contrast, when A is much higher than K (the second regime), the maximum pexsD output ($\sim$1) does not change much such that increasing A allows for the reduced response time. As expected, the response time is affected by not only K but also the protein degradation and dilution (i.e. growth) rate (Supplementary Figures S2 and S3). Our computational simulations are consistent with previous reports (12,13,15) and demonstrate that tuning the free ExsA concentration can increase or decrease response times.

Because the other protein regulators (ExsD, ExsC and ExsE) affect the target gene expression (33) (Figure 1), we hypothesized that these regulators also play important roles in modulating gene expression dynamics of the ExsADCE regulatory cascade by fine-tuning the free ExsA concentration (Supplementary Data). In a circuit that consists of ExsA and ExsD, the presence of ExsD can lower the steady-state free ExsA concentration through molecular sequestration, increasing the response time in the second regime (i.e. at high steady-state free ExsA concentrations; Figure 2C). In the same regime, our simulation showed that the response time decreases with the ExsC synthesis rate (Figure 2D). These models suggest that ExsC mediates rapid gene expression responses by sequestering ExsD and releasing free ExsA in the complex cascade. Motivated and guided by these model predictions, we systematically constructed multi-member, sequestration-based genetic circuits and experimentally characterized their gene expression dynamics in *E. coli*.

Experimentally measuring dynamics of the ExsADCE cascade

To experimentally determine the impact of ExsD on the response time, we performed time-course experiments on the simple two-member sequestration-based cascade (ExsA–ExsD; Figure 3A). The ExsD synthesis rate was varied experimentally by using three different aTc concentrations.

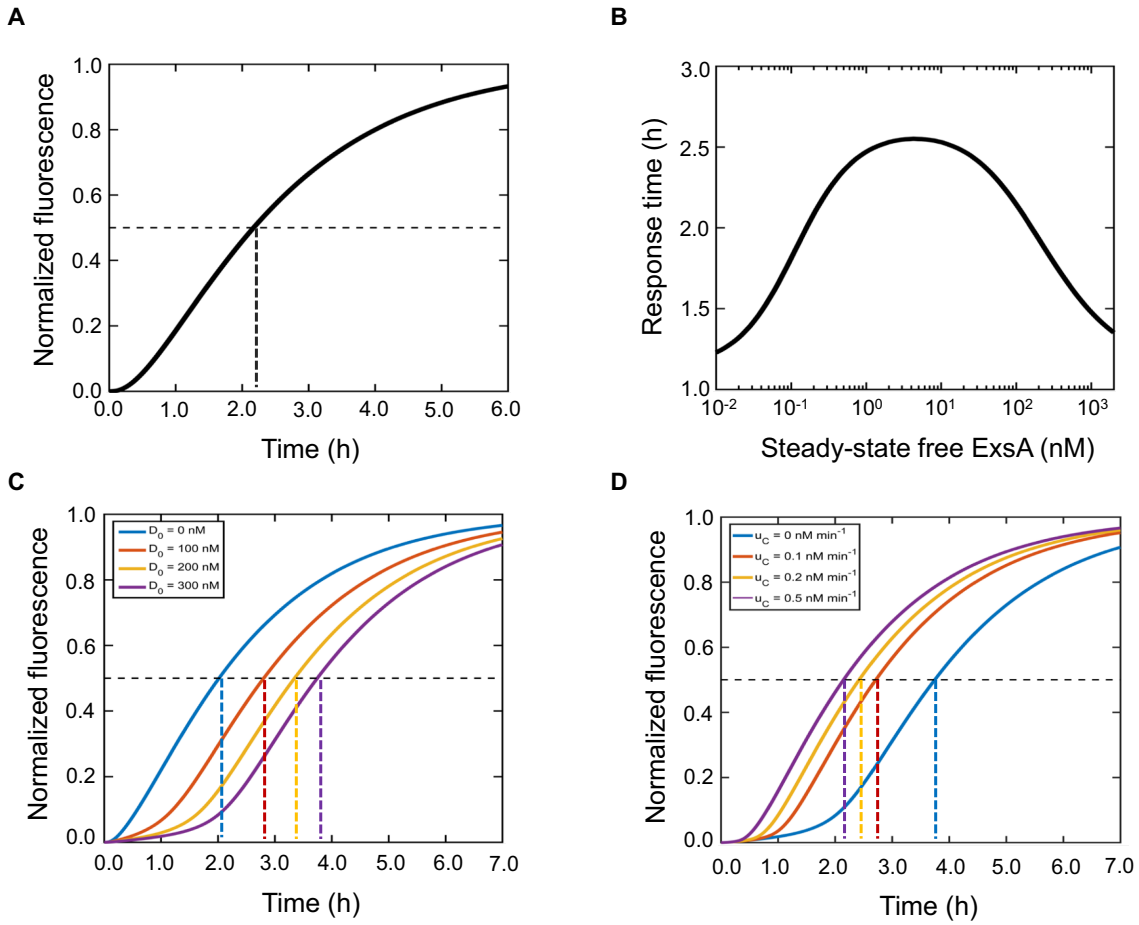

Figure 2. Modeling dynamics of the ExsADCE regulatory cascade. (**A**). Determination of the response time which is defined as the time to reach 50% of the maximum output (indicated by the dashed line). (**B**). The gene expression dynamics of the pexsD promoter depend on the steady-state free ExsA concentration. (**C**). The apparent ExsD concentration (i.e. the initial free ExsD concentration of OFF-state cells) modifies the gene expression dynamics. Four apparent ExsD (D_0) concentrations were used: 0, 100, 200 and 300 nM. (**D**). ExsC is a key regulator that mediates rapid gene expression dynamics by sequestering ExsD. Four ExsC synthesis rates were used: 0, 0.1, 0.2 and 0.5 nM/min. All model parameters and details are shown in Supplementary Data.

Our simulation (Figure 3B) and experimental data (Figure 3C and D) showed that the response time (7–10 h) increased with the ExsD synthesis rate (the aTc concentration). Comparing the model prediction with the experimental data (Figure 3E; Supplementary Data), we found that the ExsAD cascade operated in the higher ExsA concentration regime, where ExsD served mainly as a filter by sequestering ExsA and delaying the response.

Such a delayed response (up to ∼10 h) in the ExsAD cascade would not be ideal for the timely T3SS activation. We hypothesized that ExsC can speed up the response time by sequestering and inactivating ExsD. To test this hypothesis, we investigated the three-member cascade (ExsA–ExsD–ExsC; Figure 4A) by varying the ExsD (aTc) and ExsC (3OC6) synthesis rates (Figure 4B–D). While the ExsADC cascade was tested in the similar, higher ExsA concentration regime (Figure 4E and F; Supplementary Data), the response time (2–3.5 h) was significantly reduced, compared to that of the ExsAD cascade (Figure 3E). In addition, there was a significant increase in the response time ($P = 0.037$; two-tailed, unpaired, Student's t-test) between the lowest and highest aTc concentrations (0 and 100 ng/ml), and a significant decrease in the response time ($P = 0.011$) between the lowest and highest 3OC6 concentrations (0.5 and 40 nM). These results suggest that ExsC plays a role in the rapid T3SS activation by sequestering ExsD and quickly releasing ExsA from the ExsD–ExsA complex.

ExsE (anti-anti-anti-activator) was found to affect the response time in a different manner from that of ExsD (anti-activator). To determine the effect of ExsE on the response time, the entire ExsADCE cascade (Figure 5A) was characterized by varying the ExsD (aTc) and ExsE (Ara) synthesis rates at a fixed ExsC (3OC6) synthesis rate (Figure 5B–D). In the absence of ExsE (Ara = 0; Figure 5E), the response time increased monotonically with the ExsD synthesis rate. In contrast, our modeling and experimental data showed that the response time mainly decreased with the ExsE synthesis rate (Figure 5B and C), indicating that the entire ExsADCE cascade was tested mainly in the lower free ExsA concentration regime (Figure 5F). For example, we observed a significant decrease in the response time with the ExsE synthesis rate (between 0 and 25 mM Ara con-

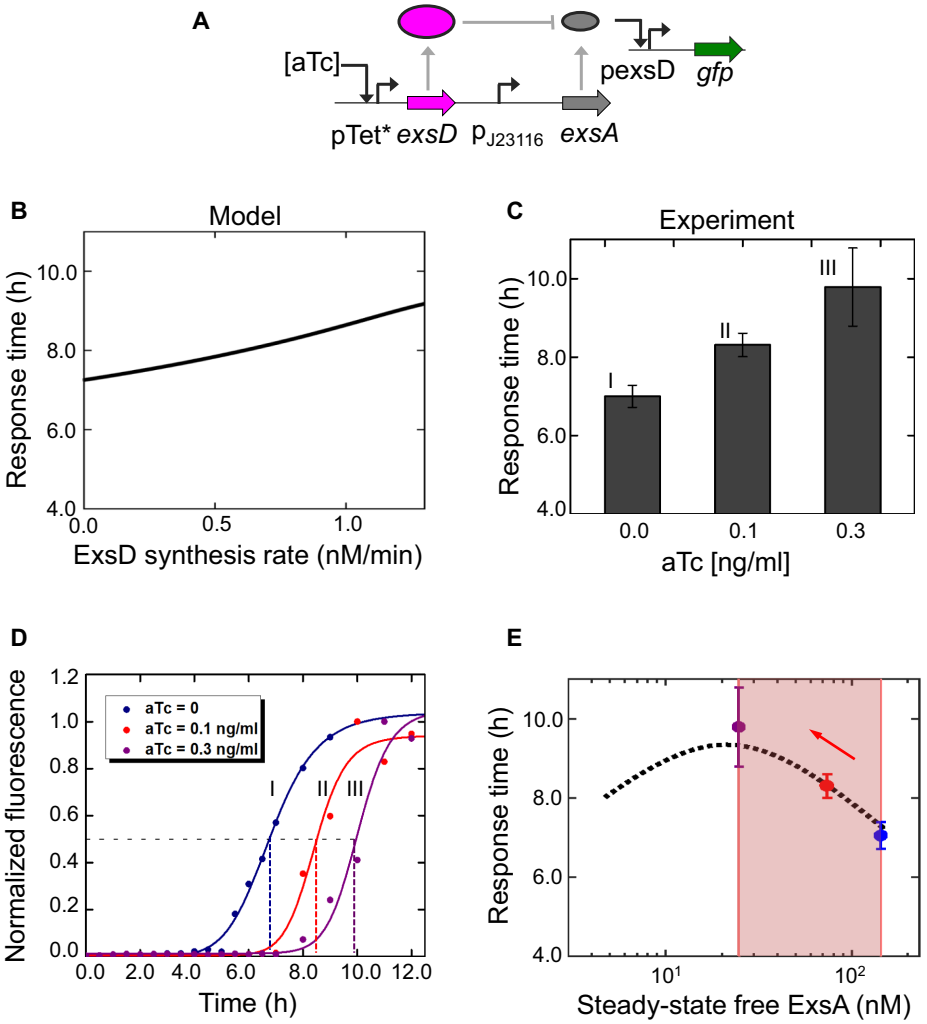

Figure 3. Dynamics of a two-member ExsAD (ExsA–ExsD) cascade. (**A**). Schematic diagram of the ExsAD regulatory cascade. (**B**). Mathematical model showing that the response time increases with the ExsD synthesis rate. (**C**). Experimental data showing that the response time increases with the aTc concentration (0, 0.1 and 0.3 ng/ml). Data and error bars respectively represent the averages and SEM of experiments performed on three different days. There is a significant increase in the response time ($P = 0.028$; two-tailed, unpaired, Student's t-test) between aTc = 0 (lowest) and aTc = 0.3 ng/ml (highest). Supplementary Figure S8A shows the corresponding, achievable maximum pexsD outputs (fluorescence in REU). (**D**) Representative time-course data corresponding to I, II, and III in Figure 3C. Each fluorescence data point is normalized to its maximum fluorescence value. The solid curves correspond to the fit to a mathematical model (Supplementary Data). (**E**). Response times over a wide range of steady-state free ExsA concentrations (with the highlighted experimental range). The dotted line represents the ExsAD circuit model prediction (Supplementary Data). For the experimental data (filled circles), the steady-state free ExsA concentrations were estimated by using the model (Supplementary Data). The arrow indicates an increasing ExsD synthesis rate.

centrations; $P = 0.028$; two-tailed, unpaired, Student's t-test). If the cascade were in the higher free ExsA concentration regime, we would expect the response time to increase with the ExsE synthesis rate through sequestration of ExsC by ExsE. As discussed earlier, when the free ExsA concentration (A) is sufficiently low, a decrease in A will require less time to reach the pexsD output of $A/2K$, leading to the reduced response time. Consistent with this explanation, it was experimentally observed that the 'achievable maximum' pexsD output decreased with the ExsE synthesis rate (or Ara concentration; Supplementary Figure S8C). These results demonstrate complex dynamic behaviors of the ExsADCE cascade that could not be understood without computational modeling and quantitative experimental characterization of synthetic circuits.

In transcriptional cascades, the response time increases with the cascade depth because the progression of the signal between layers requires slow processes, including transcription, translation, and regulator degradation (12). However, we have demonstrated that in sequestration-based regulatory cascades, longer cascades (e.g. the four-member ExsADCE cascade in Figure 5) can generate faster gene expression responses than the shorter cascade (the two-member ExsAD cascade in Figure 3) under some conditions. This is due to the fast process of protein–protein interaction and is consistent with a recent report showing that in some parameter regimes, longer regulatory cascades that combine small RNA and protein regulators can generate faster responses than shorter cascades (13). Taken together, our results showed that by controlling the synthesis rate of

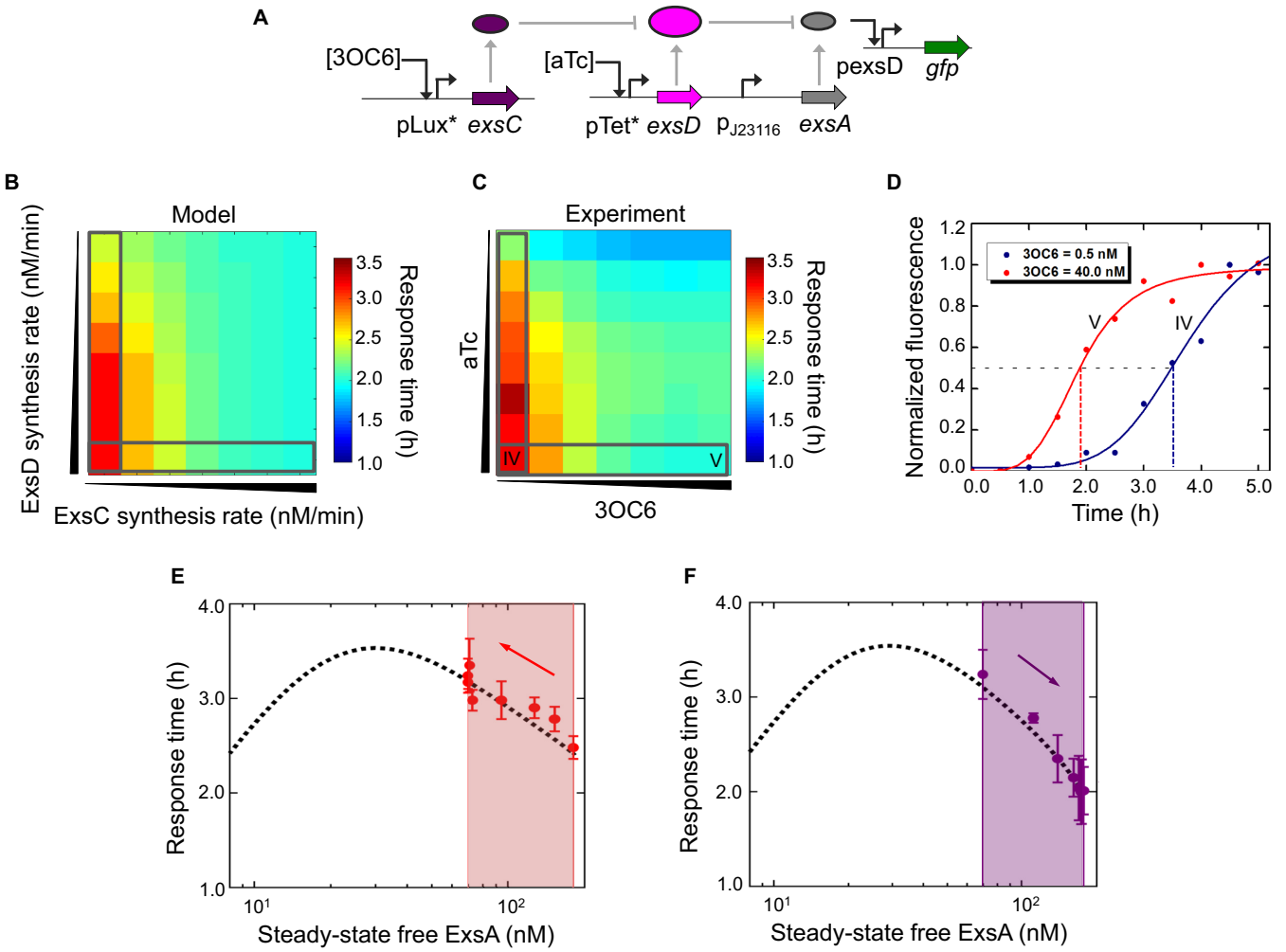

Figure 4. Dynamics of a three-member ExsADC (ExsA–ExsD–ExsC) cascade. (**A**). Schematic diagram of the ExsADC regulatory cascade. (**B**). Mathematical model showing that the response time increases with the ExsD synthesis rate, but decreases with the ExsC synthesis rate. (**C**). Experimental data showing that the response time increases with aTc (0, 0.2, 0.4, 1, 5, 10, 50 and 100 ng/ml), but decreases with 3OC6 (0.5, 1, 1.6, 3, 5, 8 and 40 nM). Data are averages of experiments performed on at least three different days. Supplementary Figure S8B shows the corresponding, achievable maximum pexsD outputs (fluorescence in REU). (**D**). Representative time-course data corresponding to IV and V in Figure 4C. Each fluorescence data point is normalized to its maximum fluorescence value. The solid curves correspond to the fit to a mathematical model (Supplementary Data). (**E** and **F**). Response times over a wide range of steady-state free ExsA concentrations (with the highlighted experimental range: the vertical gray box in Figures 4B/C is for Figure 4E; the horizontal gray box for Figure 4F). The dotted line represents the ExsADC circuit model prediction (Supplementary Data). For the experimental data (filled circles), the steady-state free ExsA concentrations were estimated by using the model (Supplementary Data). Data and error bars respectively represent the averages and SEM of experiments performed on at least three different days. The red and purple arrows respectively represent increasing ExsD and ExsC synthesis rates. There is a significant increase in the response time ($P = 0.037$; two-tailed, unpaired, Student's t-test) between aTc = 0 (lowest) and aTc = 100 ng/ml (highest). There is also a significant decrease in the response time ($P = 0.011$) between 3OC6 = 0.5 nM (lowest) and 3OC6 = 40 nM (highest).

each protein regulator, we can fine-tune the gene expression dynamics of the ExsACDE regulatory network, and that each protein plays an important role in modulating the complex dynamic behavior.

ExsD negative feedback reduces response times and enhances the robustness of ExsADCE dynamics

A transcriptional (direct) negative feedback loop is a recurring motif in natural biological networks and can reduce the response time (7). We hypothesized that indirect, sequestration-based negative feedback in the native ExsADCE regulatory network can also speed up the response time. To create an indirect negative feedback loop, we constructed a new circuit in which an additional *exsD* gene is expressed from the pexsD promoter (Figure 6A). Our computational model showed that the ExsD negative feedback (DNF) loop can decrease the response time (Figure 6B and Supplementary Figure S4). As shown in Figure 6C, the experimentally determined response times of the DNF circuit (~1.5 h) are lower than those of the 'no feedback' counterpart (2–3.5 h; Figure 4C). In addition, the DNF circuit generated gene expression dynamics that are more robust (less sensitive) to changes in regulator synthesis rates (Figure 6B and C) and changes in the free ExsA concentrations (Figure 6D and E), compared to the circuit

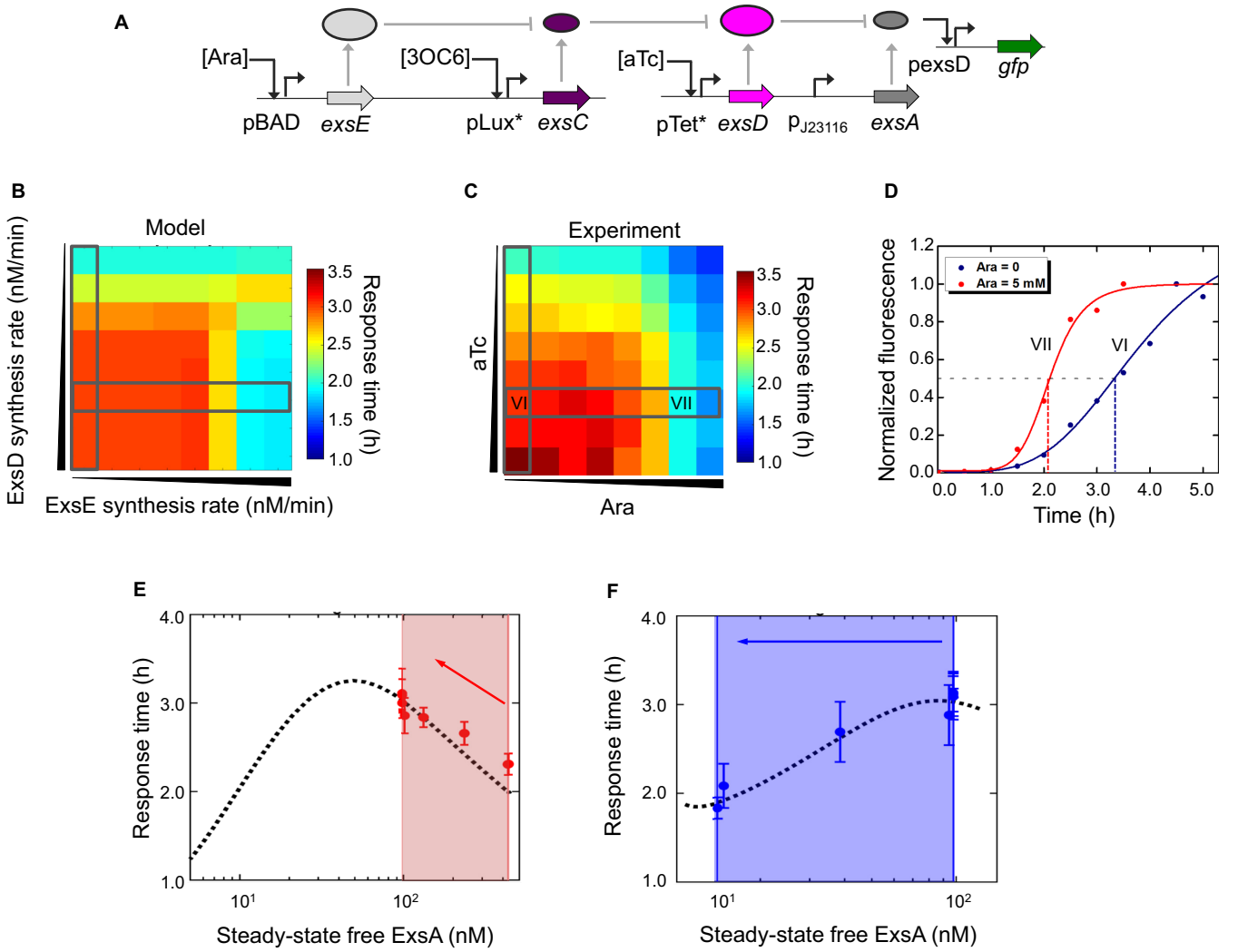

Figure 5. Dynamics of a four-member ExsADCE (ExsA–ExsD–ExsC–ExsE) cascade. (**A**). Schematic diagram of the ExsADCE regulatory cascade. (**B**) Mathematical model showing the response time as a function of ExsD and ExsE synthesis rates. (**C**) Experimental data showing the response time as a function of aTc (0, 0.2, 0.4, 1, 5, 10, 50 and 100 ng/ml) and Ara (0, 0.0016, 0.008, 0.04, 0.2, 1, 5 and 25 mM) concentrations when 1.25 nM 3OC6 was used. Data are averages of experiments performed on at least three different days. Supplementary Figure S8C shows the corresponding, achievable maximum pexsD outputs (fluorescence in REU). (**D**) Representative time-course data corresponding to VI and VII in Figure 5C. Each fluorescence data point is normalized to its maximum fluorescence value. The solid curves correspond to the fit to a mathematical model (Supplementary Data). (**E** and **F**) Response times over a wide range of steady-state free ExsA concentrations (with the highlighted experimental range: the vertical gray box in Figures 5B/C is for Figure 5E; the horizontal gray box for Figure 5F). The dotted line represents the ExsADCE circuit model prediction (Supplementary Data). For the experimental data (filled circles), the steady-state free ExsA concentrations were estimated by using the model (Supplementary Data). Data and error bars respectively represent the averages and SEM of experiments performed on at least three different days. The red and blue arrows respectively represent increasing ExsD and ExsE synthesis rates. There is a significant increase in the response time ($P = 0.044$; two-tailed, unpaired, Student's t-test) between aTc = 0 (lowest) and aTc = 100 ng/ml (highest). There is also a significant decrease in the response time ($P = 0.028$) between Ara = 0 (lowest) and Ara = 25 mM (highest).

without negative feedback. These results suggest that DNF enables robust and rapid activation of T3SS.

DISCUSSION

The *P. aeruginosa* T3SS is a complex, highly regulated nanomachine which secretes effector proteins into eukaryotic cells during pathogenesis. At its core, the intricate ExsADCE regulatory cascade (19–23) modulates temporal expression patterns of effector proteins and the needle structure components. Other complex regulatory circuits, which respond to poorly defined signals, are also integrated into the T3SS network and impact gene expression dynamics (25–29,40). This complexity makes it difficult to determine how each individual regulatory element contributes to control over gene expression dynamics of the T3SS. By building circuits in *E. coli* from the bottom-up, we have decoupled the ExsADCE regulatory cascade from the complex endogenous global network of *P. aeruginosa* and demonstrated that the multi-member protein–protein interactions enable fine-tuning of gene expression dynamics (Figures 2–5). In addition, we demonstrated that the indirect DNF loop embedded in the ExsADCE regulatory cascade speeds

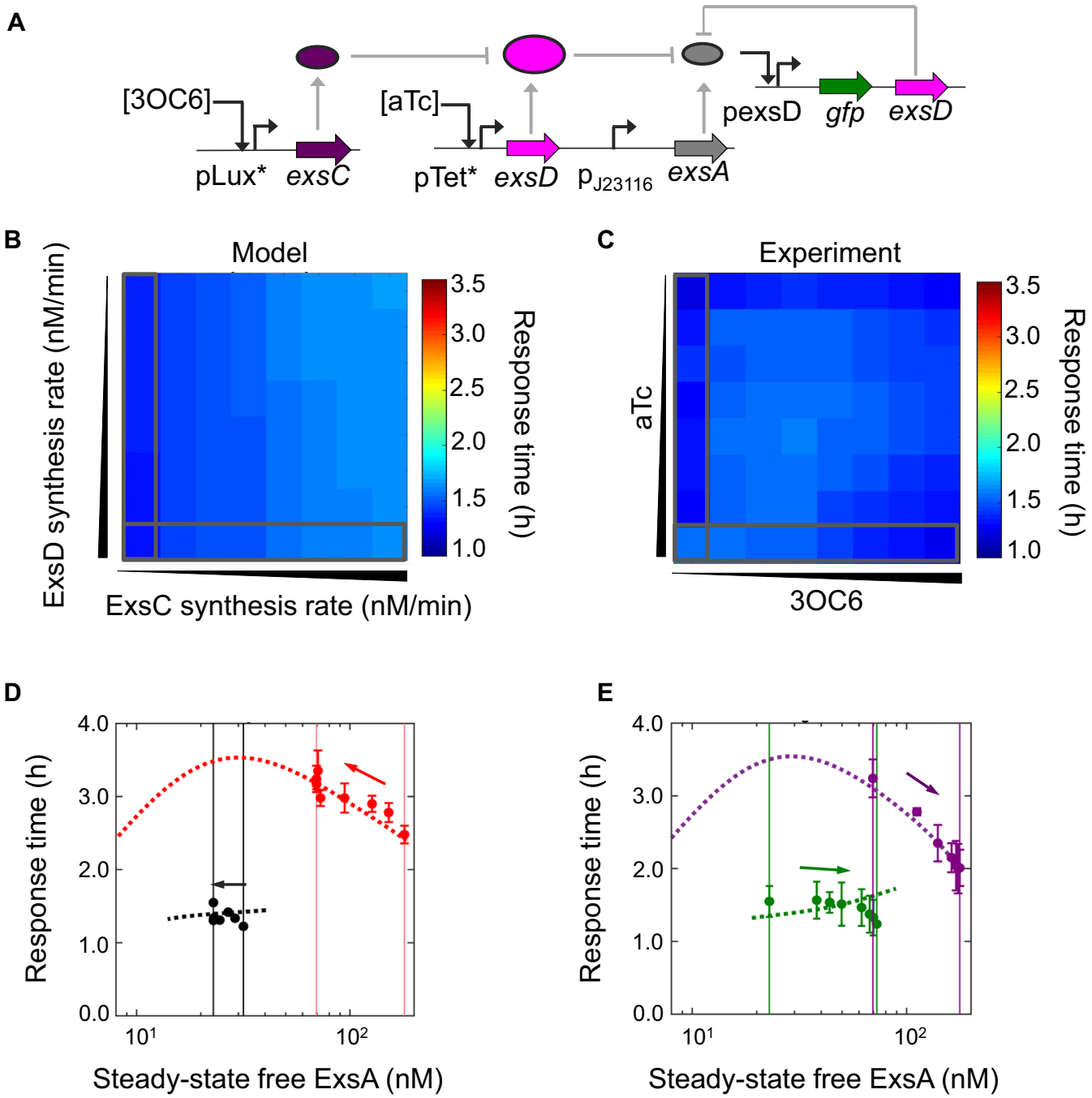

Figure 6. Indirect ExsD negative feedback decreases circuit response times and enhances the robustness of gene expression dynamics. (**A**) Schematic diagram of an ExsADC regulatory cascade containing an indirect ExsD negative feedback (DNF). (**B**) Mathematical model showing the response time as a function of ExsD and ExsC synthesis rates. Note that the same color key (response times from 1.0 to 3.5 h) is used for Figures 4–6 so that heat maps can be easily compared. When compared to Figure 4B (no feedback), Figure 6B shows that DNF leads to faster response times. (**C**) Experimental data showing the response time as a function of aTc (0, 0.2, 0.4, 1, 5, 10, 50 and 100 ng/ml) and 3OC6 (0.5, 1, 1.25, 1.6, 3, 5, 8 and 40 nM). Data are averages of experiments performed on at least three different days. Supplementary Figure S8D shows the corresponding, achievable maximum pexsD outputs (fluorescence in REU). (**D**) Response times over a wide range of steady-state free ExsA concentrations (for the vertical gray boxes in Figures 4B/C and 6B/C). Black and red points represent data from DNF and its 'no feedback' counterpart. DNF leads to faster response times and more robust gene expression dynamics (i.e. almost no changes in response times when the steady state free ExsA concentration varies) than its 'no feedback' counterpart. The dotted lines represent the model prediction (Supplementary Data). Data and error bars respectively represent the averages and SEM of experiments performed on at least three different days. Black and red arrows represent increasing ExsD synthesis rates. There is no significant increase in the response time ($P = 0.11$; two-tailed, unpaired, Student's t-test) between aTc = 0 (lowest) and aTc = 100 ng/ml (highest) in DNF (for the 'no feedback' counterpart, $P = 0.037$). (**E**) Response times over a wide range of steady-state free ExsA concentrations (for the horizontal gray boxes in Figures 4B/C and 6B/C). Green and purple points represent data from DNF and its 'no feedback' counterpart. The dotted lines represent the model prediction (Supplementary Data). Data and error bars respectively represent the averages and SEM of experiments performed on at least three different days. Green and purple arrows represent increasing ExsC synthesis rates. While small, a significant decrease in the response time ($P = 0.011$; two-tailed, unpaired, Student's t-test) was observed between 3OC6 = 0.5 nM (lowest) and 3OC6 = 40 nM (highest) in DNF.

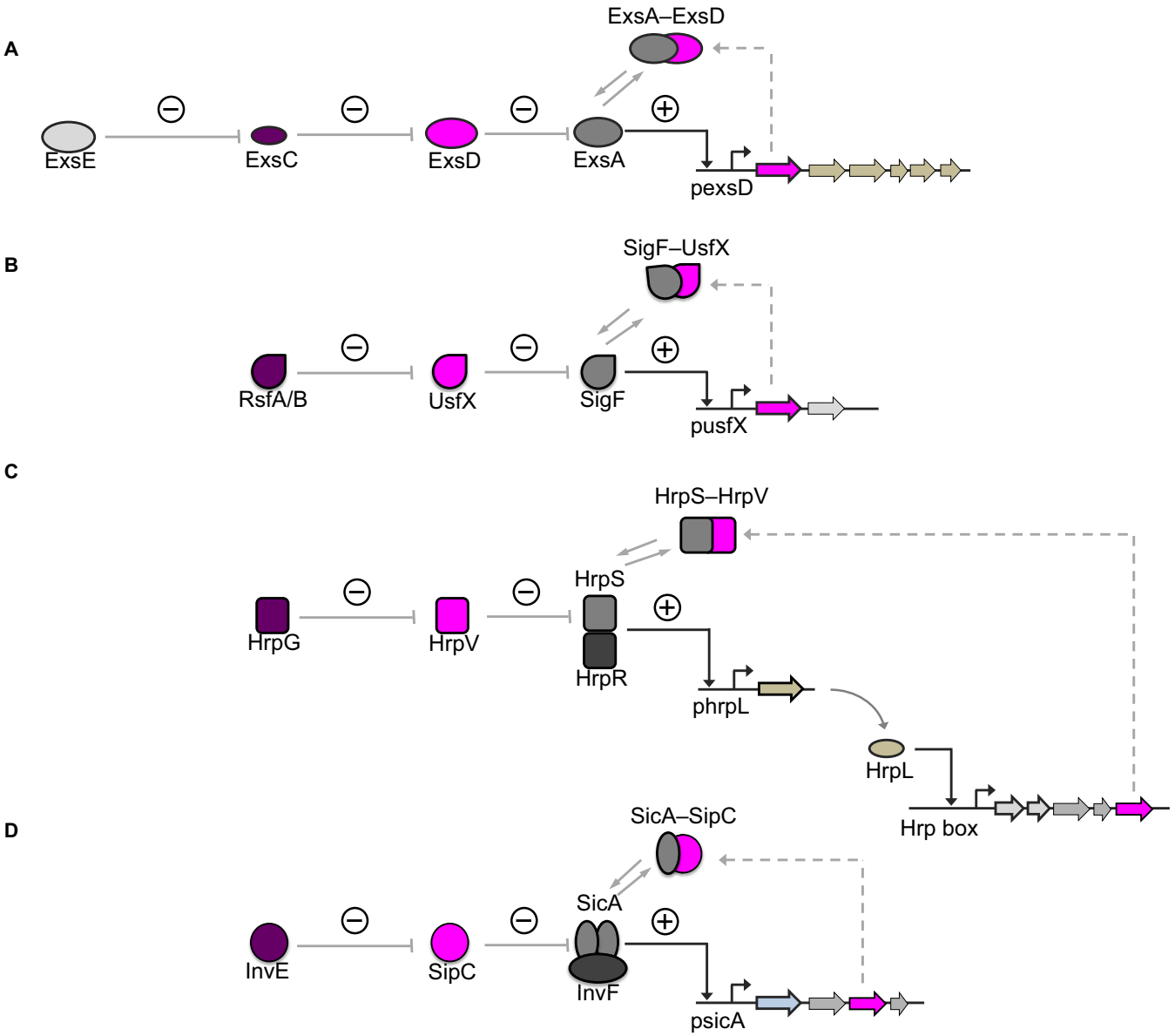

Figure 7. Gene regulatory cascades that integrate sequestration and indirect negative feedback. Sequestration-based regulatory cascades coupled with indirect negative feedback loops are found in many pathogens. (**A**) A circuit found in *Pseudomonas aeruginosa*. (**B**) A circuit found in *Mycobacterium tuberculosis*. (**C**) A circuit found in *Pseudomonas syringae*. (**D**) A circuit found in *Salmonella typhirium*. Dashed arrows represent an indirect negative feedback loop that is common across all four systems. Protein regulators that perform a similar function are indicated by the same color in each system (e.g. anti-activators in pink and anti-anti-activators in violet). For simplicity, other feedback loops and interactions are not shown.

up the circuit response time and enhances the robustness of gene expression dynamics (Figure 6). This work provides insights into the gene expression dynamics of the ExsADCE regulatory cascade, the first step toward understanding its system-level behavior and combating bacterial pathogenesis.

In this work, we have constructed and characterized the ExsADCE regulatory cascade in *E. coli*, to our knowledge, the longest protein sequestration-based circuit built so far. By combining experiments and computational modeling, we have shown that the gene expression dynamics of the ExsADCE cascade are determined by four factors: (i) the steady-state free ExsA concentration, (ii) the apparent ExsD concentration, (iii) sequestration-based multimember protein interactions in which ExsC mediates rapid response dynamics and (iv) indirect negative feedback topologies. To further investigate the effect of negative feedback, we have constructed two additional negative feedback loops: ExsE negative feedback (ENF) and combined ExsD–ExsE negative feedback (DENF). We found that both ENF and DENF produced gene expression dynamics similar to DNF (Supplementary Figures S4–S6). These results suggest that the negative feedback topology in the ExsADCE regulatory cascade may have redundant functions in which the impact on gene expression dynamics due to unexpected inactivation of one regulator is minimized by the other reg-

ulator (41,42). Taken together, our results suggest that the multiple protein interactions and indirect negative feedback loops enable the T3SS to respond to environmental signals in a fast and robust manner.

Similar to *P. aeruginosa* (Figure 7A), diverse bacterial pathogens employ a sequestration-based, multi-member strategy to either rapidly adapt to different stresses, including the immune response of the host cells, or control the T3SS activity. In *Mycobacterium tuberculosis*, an alternate sigma factor (SigF) mediates an adaptive mechanism during stresses such as antibiotic exposure (43), and contributes to the immune pathology of tuberculosis by modifying *M. tuberculosis* cell membrane properties (44). Through a direct interaction (Figure 7B), the anti-activator UsfX sequesters SigF into an inactive complex SigF–UsfX (16). An anti-anti-activator (RsfA or RsfB) sequesters UsfX through a partner-switching mechanism, which frees SigF to activate its target genes (16). Another example is the *Pseudomonas syringae* hypersensitive response and pathogenicity (*hrp*) system, which is a multicomponent cascade that regulates the T3SS (45). In the *hrp* regulatory cascade (Figure 7C), HrpR and HrpS directly interact to form a complex which activates the target promoter (46). The anti-activator HrpV sequesters HrpS and represses gene expression (17). A fourth regulator HrpG sequesters HrpV, releasing HrpS to form a complex with HrpR and activate downstream *hrp* genes (47). In the *Salmonella typhirium* T3SS (Figure 7D), a transcriptional activator InvF interacts with a chaperone SicA to form a complex that activates the *sicA* promoter (18). A third regulator SipC sequesters SicA, which prevents SicA from interacting with InvF until SipC is exported (18). A fourth regulator InvE interacts with SipC and controls its secretion (48,49). In all four systems shown in Figure 7, indirect anti-activator negative feedback loops are present (ExsD, UsfX, HrpV or SipC).

Sequestration-based genetic circuits have been relatively unexplored despite their importance in cellular processes. They play an important role in generating flexible ultrasensitive responses (15,33,50,51), and when combined with positive feedback, protein sequestration can be used to build robust, tunable bistable switches (33,36,52). Through model-guided experimental analyses, we provide insights into gene expression dynamics of the important recurring motif that consists of multiple sequestration-based interactions and negative feedback loops. Our quantitative, bottom-up approach will be useful for understanding dynamics of other complex regulatory cascades in the future.

SUPPLEMENTARY DATA

Supplementary Data are available at NAR Online.

ACKNOWLEDGEMENTS

We thank James Ballard and Allison Hoynes-O'Connor for helpful comments on the manuscript.

FUNDING

National Science Foundation [CBET-1350498]. Funding for open access charge: National Science Foundation [CBET-1350498].

Conflict of interest statement. None declared.

REFERENCES

1. Ray,J.C.J., Tabor,J.J. and Igoshin,O.A. (2011) Non-transcriptional regulatory processes shape transcriptional network dynamics. *Nat. Rev. Microbiol.*, **9**, 817–828.
2. Waters,L.S. and Storz,G. (2009) Regulatory RNAs in bacteria. *Cell*, **136**, 615–628.
3. Shimoni,Y., Friedlander,G., Hetzroni,G., Niv,G., Altuvia,S., Biham,O. and Margalit,H. (2007) Regulation of gene expression by small non-coding RNAs: a quantitative view. *Mol. Syst. Biol.*, **3**, 138.
4. Guillier,M., Gottesman,S. and Storz,G. (2006) Modulating the outer membrane with small RNAs. *Genes Dev.*, **20**, 2338–2348.
5. Takahashi,M.K., Chappell,J., Hayes,C.A., Sun,Z.Z., Kim,J., Singhal,V., Spring,K.J., Al-Khabouri,S., Fall,C.P., Noireaux,V. *et al.* (2015) Rapidly characterizing the fast dynamics of RNA genetic circuitry with cell-free transcription-translation (TX-TL) systems. *ACS Synth. Biol.*, **4**, 503–515.
6. Chappell,J., Watters,K.E., Takahashi,M.K. and Lucks,J.B. (2015) A renaissance in RNA synthetic biology: new mechanisms, applications and tools for the future. *Curr. Opin. Chem. Biol.*, **28**, 47–56.
7. Rosenfeld,N., Elowitz,M.B. and Alon,U. (2002) Negative autoregulation speeds the response times of transcription networks. *J. Mol. Biol.*, **323**, 785–793.
8. Bennett,M.R., Pang,W.L., Ostroff,N.A., Baumgartner,B.L., Nayak,S., Tsimring,L.S. and Hasty,J. (2008) Metabolic gene regulation in a dynamically changing environment. *Nature*, **454**, 1119–1122.
9. Chechik,G., Oh,E., Rando,O., Weissman,J., Regev,A. and Koller,D. (2008) Activity motifs reveal principles of timing in transcriptional control of the yeast metabolic network. *Nat. Biotechnol.*, **26**, 1251–1259.
10. Zaslaver,A., Mayo,A.E., Rosenberg,R., Bashkin,P., Sberro,H., Tsalyuk,M., Surette,M.G. and Alon,U. (2004) Just-in-time transcription program in metabolic pathways. *Nat. Genet.*, **36**, 486–491.
11. Kalir,S., McClure,J., Pabbaraju,K., Southward,C., Ronen,M., Leibler,S., Surette,M.G. and Alon,U. (2001) Ordering genes in a flagella pathway by analysis of expression kinetics from living bacteria. *Science* **292**, 2080–2083.
12. Hooshangi,S., Thiberge,S. and Weiss,R. (2005) Ultrasensitivity and noise propagation in a synthetic transcriptional cascade. *Proc. Natl. Acad. Sci. U.S.A.*, **102**, 3581–3586.
13. Adamson,D.N. and Lim,H.N. (2013) Rapid and robust signaling in the CsrA cascade via RNA-protein interactions and feedback regulation. *Proc. Natl. Acad. Sci. U.S.A.*, **110**, 13120–13125.
14. Khalil,A.S. and Collins,J.J. (2010) Synthetic biology: applications come of age. *Nat. Rev. Genet.*, **11**, 367–379.
15. Buchler,N.E. and Louis,M. (2008) Molecular titration and ultrasensitivity in regulatory networks. *J. Mol. Biol.*, **384**, 1106–1119.
16. Beaucher,J., Rodrigue,S., Jacques,P.E., Smith,I., Brzezinski,R. and Gaudreau,L. (2002) Novel Mycobacterium tuberculosis anti-sigma factor antagonists control sigmaF activity by distinct mechanisms. *Mol. Microbiol.*, **45**, 1527–1540.
17. Preston,G., Deng,W.L., Huang,H.C. and Collmer,A. (1998) Negative regulation of hrp genes in Pseudomonas syringae by HrpV. *J. Bacteriol.*, **180**, 4532–4537.
18. Darwin,K.H. and Miller,V.L. (2001) Type III secretion chaperone-dependent regulation: activation of virulence genes by SicA and InvF in Salmonella typhimurium. *EMBO J.*, **20**, 1850–1862.
19. Dasgupta,N., Lykken,G.L., Wolfgang,M.C. and Yahr,T.L. (2004) A novel anti-anti-activator mechanism regulates expression of the Pseudomonas aeruginosa type III secretion system. *Mol. Microbiol.*, **53**, 297–308.
20. Frank,D.W. and Iglewski,B.H. (1991) Cloning and sequence analysis of a trans-regulatory locus required for exoenzyme S synthesis in Pseudomonas aeruginosa. *J. Bacteriol.*, **173**, 6460–6468.
21. McCaw,M.L., Lykken,G.L., Singh,P.K. and Yahr,T.L. (2002) ExsD is a negative regulator of the Pseudomonas aeruginosa type III secretion regulon. *Mol. Microbiol.*, **46**, 1123–1133.
22. Rietsch,A., Vallet-Gely,I., Dove,S.L. and Mekalanos,J.J. (2005) ExsE, a secreted regulator of type III secretion genes in Pseudomonas aeruginosa. *Proc. Natl. Acad. Sci. U.S.A.*, **102**, 8006–8011.

23. Urbanowski,M.L., Lykken,G.L. and Yahr,T.L. (2005) A secreted regulatory protein couples transcription to the secretory activity of the Pseudomonas aeruginosa type III secretion system. *Proc. Natl. Acad. Sci. U.S.A.*, **102**, 9930–9935.
24. Diaz,M.R., King,J.M. and Yahr,T.L. (2011) Intrinsic and extrinsic regulation of type III secretion gene expression in Pseudomonas aeruginosa. *Front. Microbiol.*, **2**, 89.
25. Goodman,A.L., Kulasekara,B., Rietsch,A., Boyd,D., Smith,R.S. and Lory,S. (2004) A signaling network reciprocally regulates genes associated with acute infection and chronic persistence in Pseudomonas aeruginosa. *Dev. Cell*, **7**, 745–754.
26. Laskowski,M.A., Osborn,E. and Kazmierczak,B.I. (2004) A novel sensor kinase-response regulator hybrid regulates type III secretion and is required for virulence in Pseudomonas aeruginosa. *Mol. Microbiol.*, **54**, 1090–1103.
27. Ventre,I., Goodman,A.L., Vallet-Gely,I., Vasseur,P., Soscia,C., Molin,S., Bleves,S., Lazdunski,A., Lory,S. and Filloux,A. (2006) Multiple sensors control reciprocal expression of Pseudomonas aeruginosa regulatory RNA and virulence genes. *Proc. Natl. Acad. Sci. U.S.A.*, **103**, 171–176.
28. Wolfgang,M.C., Lee,V.T., Gilmore,M.E. and Lory,S. (2003) Coordinate regulation of bacterial virulence genes by a novel adenylate cyclase-dependent signaling pathway. *Dev. Cell*, **4**, 253–263.
29. Zolfaghar,I., Angus,A.A., Kang,P.J., To,A., Evans,D.J. and Fleiszig,S.M. (2005) Mutation of retS, encoding a putative hybrid two-component regulatory protein in Pseudomonas aeruginosa, attenuates multiple virulence mechanisms. *Microbes Infect.*, **7**, 1305–1316.
30. Durfee,T., Nelson,R., Baldwin,S., Plunkett,G. 3rd, Burland,V., Mau,B., Petrosino,J.F., Qin,X., Muzny,D.M., Ayele,M. *et al.* (2008) The complete genome sequence of Escherichia coli DH10B: insights into the biology of a laboratory workhorse. *J. Bacteriol.*, **190**, 2597–2606.
31. Engler,C., Kandzia,R. and Marillonnet,S. (2008) A one pot, one step, precision cloning method with high throughput capability. *PLoS One*, **3**, e3647.
32. Moon,T.S., Lou,C.B., Tamsir,A., Stanton,B.C. and Voigt,C.A. (2012) Genetic programs constructed from layered logic gates in single cells. *Nature*, **491**, 249–253.
33. Shopera,T., Henson,W.R., Ng,A., Lee,Y.J., Ng,K. and Moon,T.S. (2015) Robust, tunable genetic memory from protein sequestration combined with positive feedback. *Nucleic Acids Res.*, **43**, 9086–9094.
34. Hoynes-O'Connor,A., Hinman,K., Kirchner,L. and Moon,T.S. (2015) De novo design of heat-repressible RNA thermosensors in E-coli. *Nucleic Acids Res.*, **43**, 6166–6179.
35. Zheng,Z., Chen,G., Joshi,S., Brutinel,E.D., Yahr,T.L. and Chen,L. (2007) Biochemical characterization of a regulatory cascade controlling transcription of the Pseudomonas aeruginosa type III secretion system. *J. Biol. Chem.*, **282**, 6136–6142.
36. Venturelli,O.S., El-Samad,H. and Murray,R.M. (2012) Synergistic dual positive feedback loops established by molecular sequestration generate robust bimodal response. *Proc. Natl. Acad. Sci. U.S.A.*, **109**, E3324–3333.
37. Taniguchi,Y., Choi,P.J., Li,G.W., Chen,H., Babu,M., Hearn,J., Emili,A. and Xie,X.S. (2010) Quantifying E. coli proteome and transcriptome with single-molecule sensitivity in single cells. *Science*, **329**, 533–538.
38. Bernhards,R.C., Marsden,A.E., Esher,S.K., Yahr,T.L. and Schubot,F.D. (2013) Self-trimerization of ExsD limits inhibition of the Pseudomonas aeruginosa transcriptional activator ExsA in vitro. *FEBS J.*, **280**, 1084–1094.
39. Lykken,G.L., Chen,G., Brutinel,E.D., Chen,L. and Yahr,T.L. (2006) Characterization of ExsC and ExsD self-association and heterocomplex formation. *J. Bacteriol.*, **188**, 6832–6840.
40. Hauser,A.R. (2009) The type III secretion system of Pseudomonas aeruginosa: infection by injection. *Nat. Rev. Microbiol.*, **7**, 654–665.
41. Kafri,R., Springer,M. and Pilpel,Y. (2009) Genetic redundancy: new tricks for old genes. *Cell*, **136**, 389–392.
42. Kondrashov,F.A., Rogozin,I.B., Wolf,Y.I. and Koonin,E.V. (2002) Selection in the evolution of gene duplications. *Genome Biol.*, **3**, RESEARCH0008.
43. Michele,T.M., Ko,C. and Bishai,W.R. (1999) Exposure to antibiotics induces expression of the Mycobacterium tuberculosis sigF gene: implications for chemotherapy against mycobacterial persistors. *Antimicrob. Agents Chemother.*, **43**, 218–225.
44. Williams,E.P., Lee,J.H., Bishai,W.R., Colantuoni,C. and Karakousis,P.C. (2007) Mycobacterium tuberculosis SigF regulates genes encoding cell wall-associated proteins and directly regulates the transcriptional regulatory gene phoY1. *J. Bacteriol.*, **189**, 4234–4242.
45. Buttner,D. and Bonas,U. (2006) Who comes first? How plant pathogenic bacteria orchestrate type III secretion. *Curr. Opin. Microbiol.*, **9**, 193–200.
46. Xiao,Y., Heu,S., Yi,J., Lu,Y. and Hutcheson,S.W. (1994) Identification of a putative alternate sigma factor and characterization of a multicomponent regulatory cascade controlling the expression of Pseudomonas syringae pv. syringae Pss61 hrp and hrmA genes. *J. Bacteriol.*, **176**, 1025–1036.
47. Wei,C.F., Deng,W.L. and Huang,H.C. (2005) A chaperone-like HrpG protein acts as a suppressor of HrpV in regulation of the Pseudomonas syringae pv. syringae type III secretion system. *Mol. Microbiol.*, **57**, 520–536.
48. Kubori,T. and Galan,J.E. (2002) Salmonella type III secretion-associated protein InvE controls translocation of effector proteins into host cells. *J. Bacteriol.*, **184**, 4699–4708.
49. Kim,J.S., Jang,J.I., Eom,J.S., Oh,C.H., Kim,H.G., Kim,B.H., Bang,I.S., Bang,S.H. and Park,Y.K. (2013) Molecular characterization of the InvE regulator in the secretion of type III secretion translocases in Salmonella enterica serovar Typhimurium. *Microbiology*, **159**, 446–461.
50. Buchler,N.E. and Cross,F.R. (2009) Protein sequestration generates a flexible ultrasensitive response in a genetic network. *Mol. Syst. Biol.*, **5**, 272.
51. Wang,B., Barahona,M. and Buck,M. (2014) Engineering modular and tunable genetic amplifiers for scaling transcriptional signals in cascaded gene networks. *Nucleic Acids Res.*, **42**, 9484–9492.
52. Chen,D. and Arkin,A.P. (2012) Sequestration-based bistability enables tuning of the switching boundaries and design of a latch. *Mol. Syst. Biol.*, **8**, 620.